Kinetics and Mechanism of Cellulose Pyrolysis

Yu-Chuan Lin, Joungmo Cho, Geoffrey A. Tompsett, Phillip R. Westmoreland, and George W. Huber*

Department of Chemical Engineering, 159 Goessmann Laboratory, University of Massachusetts, Amherst, Massachusetts 01003-0903

Received: July 15, 2009; Revised Manuscript Received: September 17, 2009

In this paper we report the kinetics and chemistry of cellulose pyrolysis using both a Pyroprobe reactor and a thermogravimetric analyzer mass spectrometer (TGA-MS). We have identified more than 90% of the products from cellulose pyrolysis in a Pyroprobe reactor with a liquid nitrogen trap. The first step in the cellulose pyrolysis is the depolymerization of solid cellulose to form levoglucosan (LGA; 6,8-dioxabicyclo[3.2.1]octane-2,3,4-triol). LGA can undergo dehydration and isomerization reactions to form other anhydrosugars including levoglucosenone (LGO; 6,8-dioxabicyclo[3.2.1]oct-2-en-4-one), 1,4:3,6-dianhydro-β-D-glucopyranose (DGP) and 1,6-anhydro-β-D-glucofuranose (AGF; 2,8-dioxabicyclo[3.2.1]octane-4,6,7-triol). The anhydrosugars can react further to form furans, such as furfural (furan-2-carbaldehyde) and hydroxymethylfurfural (HMF; 5-(hydroxymethyl)furan-2-carbaldehyde) by dehydration reactions or hydroxyacetone (1-hydroxypropan-2-one), glycolaldehyde (2-hydroxyacetaldehyde), and glyceraldehyde (2,3-dihydroxypropanal) by fragmentation and retroaldol condensation reactions. Carbon monoxide and carbon dioxide are formed from decarbonylation and decarboxylation reactions. Char is formed from polymerization of the pyrolysis products. The pyrolytic conversion of cellulose was fitted to two different reaction models. The first model (Model I) combined the first-order kinetic model with a thermal-lag model that assumed the temperature difference between the thermocouple and specimen in TGA to be directly proportional to the heating rate. The second model (Model II) combined the first-order kinetic model with an energy balance that took into account the heat transfer at the sample boundary including the heat flow by endothermic pyrolysis reaction. Both models were able to adequately fit the empirical data. The kinetic parameters obtained from both models were similar. Cellulose pyrolysis had an activation energy of 198 kJ mol^{-1}. Model I is computationally easier, however Model II is physically more realistic. Importantly, our results indicate that the intrinsic kinetics for cellulose pyrolysis are not a function of heating rate. During the pyrolysis of cellulose a thermal temperature gradient between the cellulose and heater can occur due to the endothermic pyrolysis reaction. A faster heating rate can magnify the thermal-lag, which leads kinetic derivations to artificial outcomes.

1. Introduction

Pyrolysis-based technologies are being used for the conversion of lignocellulosic biomass into fuels and chemicals.[1−3] Pyrolysis refers to the air-free thermal decomposition, forming some combination of gases, liquids, and/or solid ("char"). Approaches for biomass conversion that involve pyrolysis include fast pyrolysis,[4−9] gasification,[10−14] and catalytic fast pyrolysis.[15,16]

Pyrolysis is typically classified in terms of heating rate and temperature.[17] Conventional ("slow") pyrolysis has been used for charcoal preparation. In contrast to slow pyrolysis, "fast" pyrolysis (higher heating rate) is a burgeoning route in the synthesis of biomass-derived liquids (bio-oils).[17] Product phases and compositions can be empirically controlled by manipulating various reaction conditions, particularly heating rates, maximum reaction temperatures, and reactant/product residence times.[18,19] Cellulose is the major component in plant tissues; therefore, understanding cellulose pyrolysis is critical in developing efficient technologies for biomass conversion using pyrolysis-based technologies. Cellulose pyrolysis is a complicated process involving multiphase reactions,[20] complex chemical pathways,[21] highly unstable intermediates,[22,23] and heat and mass transfer effects.[24−26] This topic has been studied over 60 years as summarized in Table 1.[27−52] Nevertheless, the kinetics and elementary-reaction chemistry of cellulose pyrolysis are still debated.

As shown in Table 1, there is a large variation in magnitude of the kinetic properties of cellulose and in the measurement approaches used in previous studies. The reaction kinetics for thermal decomposition of cellulose under inert atmospheres has been reported in the literature as early as 1956. Stamm et al.[27] were among the first to report an activation energy (109 kJ mol^{-1}) using Douglas fir decomposing between 383 and 493 K. In contrast, Hirata et al.[34] studied thermal decomposition kinetics of wood and of separate biomass components, including cellulose, hemicellulose, and lignin. These researchers reported two processes occurring during the thermal decomposition of cellulose: an initial reaction and a propagation reaction with activation energies of 165 and 112 kJ mol^{-1}, respectively. Possible chemical reaction mechanisms were discussed in their subsequent review paper.[53] Building on the multistep mechanism proposed by Broido and Weinstein,[54] in the late 1970s Shafizadeh and co-workers[38] developed a three-step kinetic model in which an initiation step forms "active cellulose," which subsequently decomposes by two competitive first-order reactions, one yielding volatiles and the other forming char and gas.

* Corresponding author. Fax: +1 413 545 1647; e-mail: huber@ecs.umass.edu.

10.1021/jp906702p CCC: $40.75
Published on Web 10/22/2009

TABLE 1: Selected Kinetic Studies of Cellulose Pyrolysis

material	reaction condition, temperature range, and heating rate	E_A (kJ mol^{-1})	pre-exponential factor (s^{-1})	reaction order	ref
cellulose from Douglas fir	383−483 K	109			27
cotton		175.7	5.6×10^{18}	1	28
α-cellulose		147	6.5×10^{10}		29
		234	4×10^{17}		
cellulose		209.2		1	30
cellulose Whatman no. 1 filter paper		148			31
cellulose		126	7×10^{7}		32
		234	4×10^{17}		
α-cellulose		80	1.7×10^{4}		33
cellulose	initial reaction	165	2.25×10^{7}	1	34
	propagation reaction	112			
α-cellulose		57	1.8×10^{2}		35
		48	1.8×10^{2}		
filter paper		139	6.8×10^{9}	1	36
cellulose		227	3×10^{16}		37
		167	4×10^{11}		
cellulose	cellulose to active cellulose	243	2.8×10^{19}		38
	active to volatiles	198	3.2×10^{14}		
	active to char	153	1.3×10^{10}		
filter paper	2.16 K min^{-1}	221.1	3.3×10^{15}		39
	5.65 K min^{-1}	157.6	1.4×10^{10}		
	10.9 K min^{-1}	148.8	2.7×10^{9}		
	22.4 K min^{-1}	162.6	4.5×10^{10}		
	55.0 K min^{-1}	153.0	7.0×10^{9}		
cellulose	383−873 K dynamic TGA	153	7.0×10^{9}	0.90 conversion	39
filter paper 0.0101 cm thick		132.8	2.0×10^{8}	1	40
cellulose	373−1273 K screen heater	133	1.99×10^{8}	0.94 conversion	40
Avicel cellulose		234	3.7×10^{17}	1.2	41
cellulose	2−3 mg, 2−80 K min^{-1}	228	6.3×10^{16}		42
cellulose		257	1.58×10^{20}		43
Whatman no. 6 filter paper	3−4 mg, 5, 10, 50 K min^{-1}	217.2	5.0×10^{15}	1	44
cellulose (Whatman CF-11)	30 mg, 1−60 K min^{-1} <327 °C	218	1.58×10^{16}	0−1	45
cellulose (Whatman CF-11)	$T > 600$ K	140−155	$\sim 10 \times 10^{9}$	0−1	45
cellulose (Sigma)	323−773 at 10 K min^{-1} TGA	242	6.3×10^{20}		46
cellulose (Whatman CF-11)	9 mg, 65 K min^{-1}	174	1.26×10^{11}	1	47
cellulose (Whatman CF-11)	0.3 mg, 65 K min^{-1}	209	3.16×10^{14}	1	47
cellulose (Whatman CF-11)	0.3 mg, 1 K min^{-1}	249	3.18×10^{18}	1	47
cellulose	826−896 K	82.7	4.69×10^{5}	1	48
cellulose	896−946 K	282.0	1.33×10^{23}	2	48
cellulose	1.1 mg, 65 K min^{-1}	213	2.51×10^{15}		49
cellulose (Whatman 41 filter paper)	hydroxyacetaldehyde, formaldehyde and CO formation	198			50
	tars and CO_2 formation	148			
cellulose	transglycosylation	190−200			51, 52
	elimination	250			

This empirical Broido−Shafizadeh model has been widely accepted but does not describe the decomposition mechanism in detail. Suuberg and co-workers[45,55,56] observed a transition in activation energy from >200 to 140 kJ mol^{-1} at about 600 K, attributing the lower number to evaporation of tars. In 1998, Antal and collaborators[47] found a first-order rate law with a high activation energy (228 kJ mol^{-1}) for pure cellulose at both low and high heating rates, claiming that a universal rate law had not been observed because of thermal-lag (temperature deviation between external environment and intrinsic sample), interfering with measurement of kinetics.[47]

Heating rate in cellulose pyrolysis has been shown to have an effect on the product distribution, but this aspect has been poorly understood.[45,57] For the purpose of making liquid and/or gaseous products, rapid heat input is desired (i.e., fast pyrolysis); in contrast, solid products are mostly prepared using slow heating rates.[3,58] It is generally accepted that pyrolysis chemistry and thermal transfer resistance are strongly influenced by heating rates.[24,47,59−61] An excellent summary reported by Milosavljevic and Suuberg[45] showed diverse kinetic parameters derived by various groups based on different heating rates. In general, the higher the heating rates, the lower the activation energy for cellulose pyrolysis was found. This effect has been mostly attributed to heat-transfer limitations.[62] Disregard of heat demand during highly endothermic fast pyrolysis can result in apparatus-specific kinetics.[24]

Identifying the elementary-reaction mechanism is now a feasible goal, where specific reaction classes and determination of products and intermediates will be important. Using molecular-beam mass spectrometry and Principal Component Analysis, in 2001 Brown, Dayton, and Daily correlated sets of peaks in the mass spectra as being associated with primary or secondary products.[7] More recently, Mamleev et al.[20,51,52] confirmed the conclusion of Shafizadeh and Bradbury[63] that the thermal decomposition of cellulose is essentially the same in both air and nitrogen over a wide range of mass loss. A two-step kinetic model was proposed to explain all observable phenomena related to the pyrolysis of cellulose, describing mass

TABLE 2: Proximate Analysis, Elemental Analysis, and Major Mass Ions Detected by MS from Cellulose Pyrolysis[a]

proximate analysis (wt %)			elemental analysis (wt %)			MS detected ions (wt %)					
volatile	fixed C	ash	C	H	O[b]	H_2(2)	CH_4(16)	H_2O(18)	CO/C_2H_4(28)	CO_2(44)	recovery[c]
94.8	5.1	0.1	43.0	6.3	50.7	0.8	0.7	8.1	12.7	19.3	41.8

[a] Noted that proximate analysis and MS detected ions were conducted at a heating rate of 15 K min^{-1}; MS detected ions, 150 K min^{-1}. [b] By balance. [c] Weight percentage of mass detected via MS, excluding char.

loss by two competing pathways of cellulose degradation, transglycosylation with $E_{tar} = 190-200$ kJ mol^{-1} and elimination with $E_{gas} = 250$ kJ mol^{-1}.

The objective of this study is to measure the intrinsic kinetics for cellulose pyrolysis to levoglucosan (6,8-dioxabicyclo[3.2.1]octane-2,3,4-triol). Intrinsic kinetic data were obtained by combining material balances with energy balances and fit to a first-order rate constant model. This intrinsic kinetic model is the first step in developing a more complex model for lignocellulosic biomass pyrolysis based on elementary-reaction kinetics. The major pyrolysis products were identified. Based on these outcomes, a plausible pathway for cellulose pyrolysis is proposed.

2. Experimental Section

All the reactants, solvents, and internal standards were used as received. These chemicals are as follows: cellulose (microcrystalline cellulose with 50 μm average particle size, Acros), levoglucosan (99%, Aldrich), levoglucosenone (6,8-dioxabicyclo[3.2.1]oct-2-en-4-one, 98%, Carbosynth), hydroxymethylfurfural (5-(hydroxymethyl)furan-2-carbaldehyde, 99%, Acros), furfural (furan-2-carbaldehyde, 99%, Acros), acetic acid (glacial, Fisher), hydroxyacetone (1-hydroxypropan-2-one, 99%, Acros), glyceraldehyde (2,3-dihydroxypropanal, 90%, Acros), glycolaldehyde dimer (1,4-dioxane-2,5-diol, crystalline, Aldrich), and methanol (99%, Fisher). Elemental analysis (C, H, and O, listed in Table 2) of cellulose was performed by Galbraith Laboratories using combustion, GLI method # ME-2. The crystallinity of the cellulose was measured to be 81% as determined from X-ray diffraction using the method of Focher et al.[64]

The analytical configuration integrated small-sample pyrolysis (Model 2000 Pyroprobe, CDS Analytical Inc.) with gas chromatography−mass spectrometry (GC-MS; Hewlett-Packard 5890 and 5972A; with Restek Rtx-5sil MS capillary column). Detailed description about the Py-GC-MS setup can be found elsewhere.[15,16] Briefly, cellulose powder was packed inside the quartz tube probe, and pyrolysis was carried out at a 150 K min^{-1} heating rate. Around 4 to 5 mg of cellulose was packed inside the probe for each trial. Cellulose particle diameters are within 140 to 325 mesh (110 to 50 μm). After reaching the designated temperature (1073 K), the probe was maintained isothermally for 240 s. The outcomes from the Py-GC-MS system provide the quantification of gaseous products, including carbon monoxide and carbon dioxide.

A liquid-nitrogen trap was employed to collect the volatiles and heavy pyrolysis products, including tar. The trap was assembled from a 25 mL Pyrex vial, a screw-tight frame with plug-valve controlled gas inlet and outlet, and the Pyroprobe pyrolyzer. A 1/4 in. channel allows the Pyroprobe to be inserted from the top of frame into the center of vial. Prior to each trial, the vial was flushed with ultrahigh purity helium (UHP He, 99.99%) with a 50 mL min^{-1} flow rate for 10 min. After being purged, the vial was made airtight by closing the outlet and inlet. The trap was then transferred in a Dewar flask with liquid nitrogen bath at 77 K, which allows rapid quenching of volatiles. Cellulose pyrolysis was carried out with the same temperature program as used in the Py-GC-MS system for the quantification of condensable volatile species which exclude gaseous species such as carbon monoxide and carbon dioxide from pyrolyzed compounds. After pyrolysis, the sealed vial was brought back to room temperature. The eluent (described later) was immediately injected into the vial, followed by vigorous rinsing for about 3 minutes. Trapped species were analyzed by both GC-MS (Shimadzu GC-2010 and QP2010S, analytes separated by Restek RTX-VMS) and high-performance liquid chromatography−mass spectrometry (HPLC-MS; Agilent 1100 LC system with Bruker Esquire-LC Ion Trap MS). For those species analyzed by GC-MS, the trapped exhausts were eluted with 1 mL of methanol; for those analyzed by HPLC-MS, 4 mL of 0.05 M sulfuric acid solution was used as eluent. HPLC-MS speciation was conducted in the Mass Spectrometry Center, University of Massachusetts−Amherst. Sulfuric acid solution (0.05 M) was used as the mobile phase with a 0.6 mL min^{-1} flow rate. An ion-exclusion column (Aminex HPX-87H, 300−7.8 mm) was employed under a working pressure of 6.2 bar at 303 K. The MS analysis was carried out with a capillary exit voltage at 140 V.

Thermogravimetric analysis (TGA), derivative thermogravimetric (DTG), and differential scanning calorimetry (DSC) data were acquired using a TA Instruments SDT Q600 system with 1, 15, and 150 K min^{-1} heating rates from 323 to 1073 K. Helium (UHP) was used as the sweep gas with a 100 mL min^{-1} flow rate. Approximately 6 to 9 mg of cellulose was consumed per trial in an alumina crucible. All solid feedstocks were sieved to obtain particle diameters between 140 to 325 mesh (110 to 50 μm). The volatile portion was measured by pyrolyzing the samples with a 15 K min^{-1} heating rate from 323 to 1073 K, followed by a 1073 K isothermal hold for 240 s. Ash was determined with the same temperature program but with ~10% of oxygen in helium as the sweep gas (100 mL min^{-1}). A quadrupole mass spectrometer (Extorr XT 300) was coupled to the SDT Q600 to analyze the exhaust during pyrolysis with an electron ionization voltage at 27 eV. The interface was wrapped with heating tape, maintained at 523 K to circumvent condensation of exhausting gases.

3. Numerical Modeling of TGA Results

In a TGA measurement, the actual sample temperature (T_s), which is directly related to the degree of pyrolysis, may differ from the external temperature (T_e) by a thermal-lag (ΔT_{TL}):

$$\Delta T_{TL} = T_e - T_s \quad (1)$$

where T_e is normally increased at a constant heating rate, β:

$$T_e = T_0 + \beta t \quad (2)$$

T_s is assumed to be uniform within the sample.

The pyrolysis of cellulose is assumed to be governed mainly by a first-order irreversible conversion of initial mass such that

subsequent steps are relatively fast. A more detailed reaction mechanism will be discussed later. This rate equation is given as:

$$\frac{d\alpha}{dt} = k(1 - \alpha) \tag{3}$$

where α is the fraction of mass involved in the pyrolysis, and an Arrhenius rate constant, k, is assumed, dependent only on T_s:

$$k(T_s) = k_0 \exp\left(-\frac{E_A}{RT_s}\right) \tag{4}$$

where k_0 and E_A are rate parameters which are assumed to be constants for any dynamic and system variables.

In order to relate these temperatures during the pyrolysis, two numerical approaches to the thermal-lag properties are considered, described below as Model I and Model II.

3.1. Model I. In Model I, the pyrolysis of cellulose is delayed by an inherent thermal delay of the apparatus. The thermal-lag is considered to be directly proportional to the heating rate ($\Delta T_{TL} = C\beta$). The sample temperature of eq 1 can be rewritten as:

$$T_s = T_0 + \beta(t - C) \tag{5}$$

where C is a proportionality factor which can be experimentally determined by fitting the experimental data to the model. The observed correction factor is $C = 0.131$ min for the current study. The same thermal-lag model has been used by Monasse and Haudin[65] ($C = 0.107$ min) for the crystallization of polypropylene and long-chain alkanes (C_nH_{2n+2} with $21 \leq n \leq 25$) at a constant cooling rate. The Runge−Kutta method is used to integrate eq 3 numerically subject to the following initial condition:

$$\alpha = 0 \quad \text{at} \quad t = 0 \tag{6}$$

3.2. Model II. The second model is based on the energy balance equation that was used by Narayan and Antal.[24] In their model, the detailed heat transfer between sample and furnace is included. In this case, it is assumed that the temperature is uniformly distributed inside the sample. The energy balance between sample and external temperature is given by

$$hA_r(T_e - T_s) = m_0(1 - \alpha)c_p\frac{dT_s}{dt} + m_0\frac{d\alpha}{dt}\Delta H \tag{7}$$

where h is the heat transfer coefficient, A_r is the average surface area for sample particles, m_0 is the initial mass of the moisture-free sample measured at initial drying temperature, T_0, and ΔH is the heat of pyrolysis. In the numerical model, observed ΔH values are used to minimize the systematic errors of correlation with experimental data. Thermal and physical parameters employed in this model are summarized in Table 3.

In order to obtain the solution for T_s and α, the coupled ordinary differential eqs 3 and 5 must be solved subject to the following initial condition:

$$\alpha = 0 \quad \text{and} \quad T_s = T_0 \quad \text{at} \quad t = 0 \tag{8}$$

TABLE 3: Parameters Employed in the Numerical Model

property	value		
T_0 (K)	400		
T_f (K)	1000		
c_p (J kg^{-1} K^{-1})	1670		
hA_r (J s^{-2} K)	2.25×10^{-3}		
	data set 1	data set 2	data set 3
β (K s^{-1})	1.667×10^{-2}	0.25	2.5
m_0 (kg)	7.43×10^{-6}	8.61×10^{-6}	5.64×10^{-6}
ΔH (kJ kg^{-1})	200	213	194

The second ordinary differential equation causes a singular boundary-value problem when the conversion approaches unity. In order to resolve the singular boundary behavior in the numerical integration, Gear's method of backward differentiation was used.

3.3. Parameter Estimation. Reaction parameters for cellulose pyrolysis are estimated by comparing the kinetic models with thermogravimetric data at different heating rates. All experimental data points from three different heating rates (highest, middle, and lowest values in the instrument limits) are included, minimizing error between experimental data and the kinetic models by adjusting pre-exponential factor and activation energy. In order to avoid numerical divergence and to consider minimal error equally distributed over each data set, irrespective of the numbers of data points, the reaction parameters are estimated by minimizing the object function based on relative area error to parametric domain as:

$$F = \frac{\sum_{i=1}^{M}\int_{T_0}^{T_f}|\alpha_i^{exp} - \alpha_i^{calc}|dT}{T_f - T_0} \tag{9}$$

where subscript i and M denote index and total number for different heating rates included in minimization, respectively. The trapezoidal rule can be applied to evaluate the integral term in the above equation.

$$F \approx \frac{\sum_{i=1}^{M}\sum_{j=1}^{N-1}(T_{i,j+1} - T_{i,j})(|\alpha_{i,j+1}^{exp} - \alpha_{i,j+1}^{calc}| + |\alpha_{i,j}^{exp} - \alpha_{i,j}^{calc}|)}{2(T_f - T_0)} \tag{10}$$

In the above equation, j designates the recorded data points. The total number of collected data points (N) are 12750, 5000, and 500 for $\beta = 1$, 15, and 150 K min^{-1}, respectively. The Nelder−Mead simplex method is used to search for the minimum point in the parametric domain and standard errors for estimated parameters. The residual values of solution and object function are used for the convergence test ($||\Delta\alpha|| \leq \varepsilon_1$ and $||\Delta\mathbf{F}|| \leq \varepsilon_2$). The convergence was typically obtained with about 100 iterations for $\varepsilon_1 = \varepsilon_2 = 1 \times 10^{-6}$, and the resulting correlation values and their corresponding standard errors of parameter adjustment are listed in Table 4.

4. Results

4.1. Chemical Evaluation. Table 2 summarizes the elemental analysis, approximate analysis, and selected MS-detected ions from cellulose pyrolysis. Around 95 wt % of cellulose can be volatilized with small amounts of fixed carbon. The elemental analysis shows a molar formula of cellulose used as ap-

TABLE 4: Estimated Kinetic Parameters for Cellulose Pyrolysis

current work	$k_0 \times 10^{-14}$ (s^{-1})	E_A (kJ mol^{-1})	overall F residue[b]
Model I	6.46 ± 0.01[a]	198.91 ± 0.02	0.024
Model II	5.51 ± 0.82	198.02 ± 0.71	0.041

previous work	$k_0 \times 10^{-14}$ (s^{-1})	E_A (kJ mol^{-1})	fitting parameters
Bradbury et al. (1979)[38]	3.17	197.90	$k_{0,v}$ and E_v[c]
Cooley et al. (1988)[66]	2.63	191	fixed k_0 and E_A
Antal et al. (1998)[47]	2.69	195	fixed k_0 and E_A
	$O(k_0) \sim$ 17 to 18	245	fixed E_A
Banyasz et al. (2001)[50]	1.7	198.74	$k_{0,v}$ and E_v

[a] 95% confidence interval for the adjusted parameter. [b] The object function value at the convergence. [c] k_v for a path of 'active cellulose to volatile' in the Broido−Shafizadeh (B−S) model.

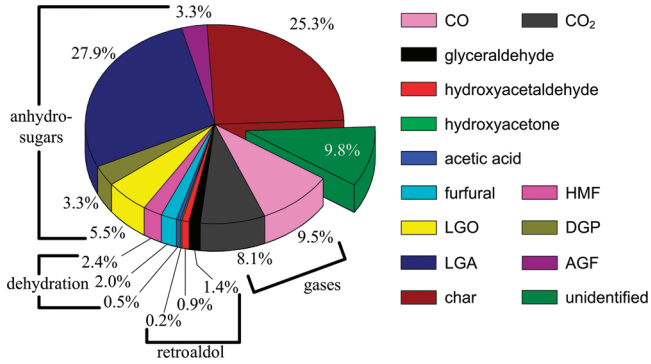

Figure 1. Carbon yields of cellulose pyrolysis from Py-GC-MS at a heating rate of 150 K min^{-1}.

proximately $(C_6H_{10}O_5)_n$. Water and carbon oxides are the major species identified by the TGA-MS.

Figure 1 shows the detailed quantitation of cellulose pyrolysis products. Besides carbon oxides and char, retroaldol products (including glyceraldehyde, hydroxyacetaldehyde, and hydroxyacetone), dehydrated species (including furfural and 5-HMF), and anhydro-monosaccharides (including levoglucosenone (LGO), 1,4:3,6-dianhydro-α-D-glucopyranose (DGP), levoglucosan (LGA), and 1,6-anhydro-β-D-glucofuranose (AGF)) are the major identified products. Quantitation of all these species was performed by interpolated calibration, injecting a standard solution of each species, except hydroxyacetaldehyde, DGP and AGF. These three are not commercially available. The calibration of hydroxyacetaldehyde was carried out by dissolving glycolaldehyde dimer (1,4-dioxane-2,5-diol) in designated amount of water. The resulting solution is then used as standard solution of hydroxyacetaldehyde. The calibrations of both DGP and AGF were based on assuming the same responses as LGA.

By using HPLC-MS, the trapped volatiles showed the presence of molar masses including 347, 509, 671, 833, 922, 995, and 1157. These heavy molecules are deemed to be the unidentified carbons (9.8%, shown in Figure 1), which cannot be detected by GC-MS. According to Lédé and co-workers,[22] these masses corresponded to ionized anhydro-oligomers. By degree of polymerization (DP), these species would be cellobiosan (DP2), cellotriosan (DP3),..., and septaosan (DP7).

Figure 2 shows the DTGs of normalized cellulose weight for different particle sizes, sweep gas flows, and initial masses at the highest heating rate (150 K min^{-1}) in this study. The overlapping curves in Figure 2a and 2b indicate negligible internal-thermal and external-mass transfer limitations. Figure 2c shows that the initial weights do affect the pyrolysis outcomes, indicating some heat transfer effects at high mass loadings. The DTGs show about 10° shift from the lightest to heaviest initial weights. In addition, the shape of the peak was

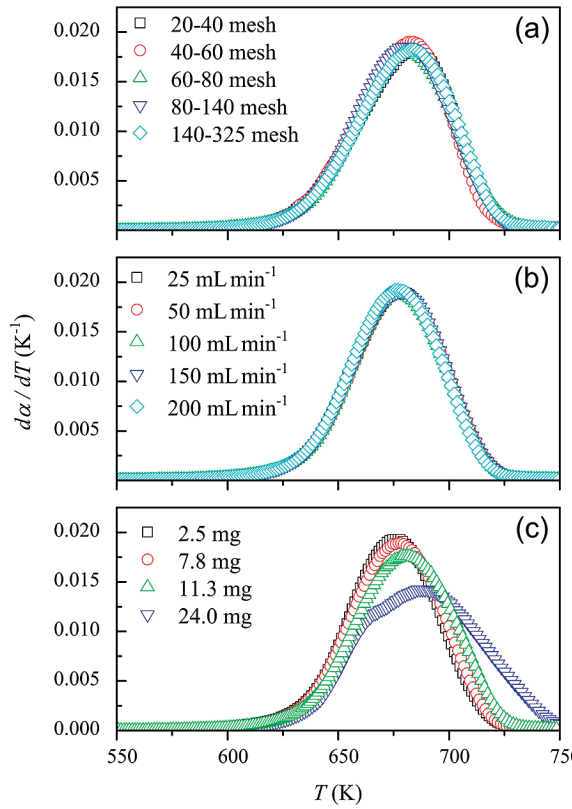

Figure 2. Cellulose pyrolysis as a function of (a) particle sizes, (b) sweep gas flow rates, and (c) initial cellulose masses at a heating rate of 150 K min^{-1}.

slightly distorted at the heaviest loading. To circumvent such influences, all the trials in this study used sample weights within a 6 to 9 mg regime.

Figure 3a and 3b illustrate the TGA and DTG outcomes of cellulose pyrolysis with 1, 15, and 150 K min^{-1} heating rates:

1. Initiation of cellulose pyrolysis happened at around 500, 550, and 600 K for heating rates of 1, 15, and 150 K min^{-1}, respectively.

2. DTG curves of all pyrolysis rates were symmetric with the fastest weight losses (DTG peaks) at 580, 624, and 682 K. The peak height decreased and the half-height width increases with increasing heating rates.

3. The residual solid from cellulose pyrolysis increased with declining heating rates, as shown in Figure 3a.

4. Figure 3c shows three endothermic peaks recorded by DSC. The heats of pyrolysis were also measured, indicated above their designated DTG peaks in Figure 3b. Two small endothermic peaks were found at around 475 K for heating-rate conditions of 1 and 15 K min^{-1}. These peaks most likely are due to the heat of cellulose decrystallization.

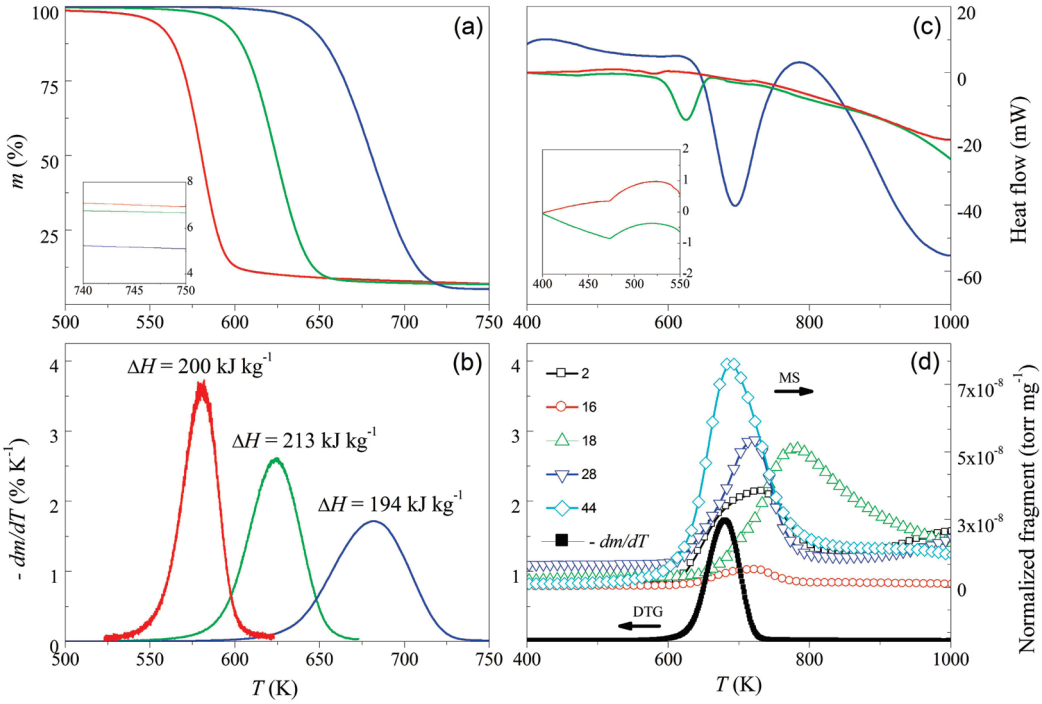

Figure 3. (a) TGA-, (b) DTG-, and (c) DSC-curves of cellulose pyrolysis at 1 K min^{-1} (red), 15 K min^{-1} (green), and 150 K min^{-1} (blue) heating rates. (d) MS responses of selected ions and DTG at a heating rate of 150 K min^{-1}.

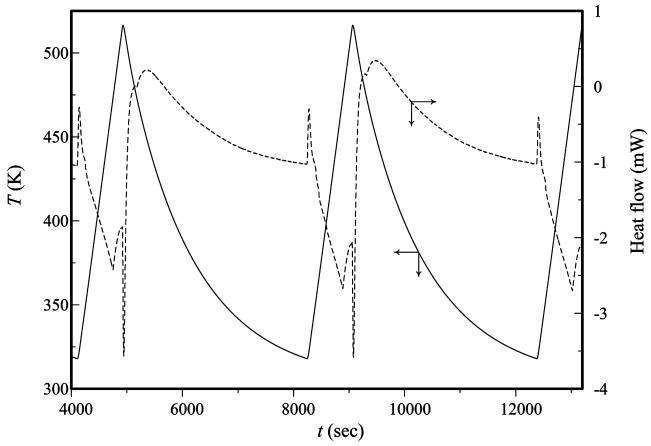

Figure 4. A three-cycle thermal treatment (323 to 523 K) of cellulose pyrolysis. Solid line represents furnace temperature (K); dash line, heat flow (mW).

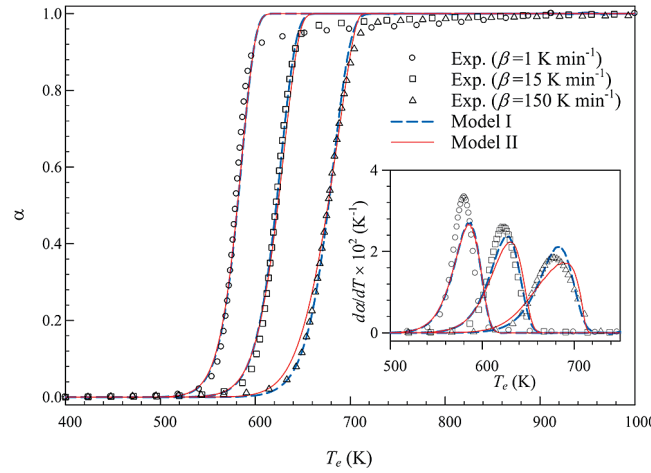

Figure 5. Measured and estimated conversions of cellulose at different heating rates.

5. Figure 3d shows the DTG-MS results at a 150 K min^{-1} heating rate. For lower heating rates (1 and 15 K min^{-1}), the MS responses of exhaust gases are not detectable.

6. Recorded ion fragments at 150 K min^{-1} included hydrogen (m/z = 2), methane (m/z = 16), water (m/z = 18), carbon monoxide and ethylene (m/z = 28), and carbon dioxide (m/z = 44). Interestingly, the onset temperatures of the species responses are in the following order: CO_2 (500 K) before CO/C_2H_4 and H_2 (600 K) before H_2O and CH_4 (620 K).

To understand the thermal behavior of the initial endothermic peak at 475 K shown in Figure 3c, a three-cycle heat treatment of cellulose was carried out, shown in Figure 4. The sample was predried at 383 K for 30 min, followed by ramping from 323 to 523 K with a 15 K min^{-1} heating rate. After reaching 523 K, the sample was cooled back to 323 K immediately. This procedure was conducted for three consecutive trials. The endothermic peak height did not change during this cycle, suggesting that this initial thermal process with cellulose is reversible. However, no reverse exothermic peak was detected, probably overshadowed during cooling process.

4.2. Effect of Thermal-Lag. To evaluate the inherent thermophysical properties of our-own TGA-DSC instrument, evaporation of naphthalene was been carried out to confirm the thermal-lag behaviors under the same conditions (1, 15, and 150 K min^{-1}) used in cellulose pyrolysis. In this test, similar thermal-lag patterns to cellulose pyrolysis were observed. A high heating rate (150 K min^{-1}) induced a significant delay in vaporization. Although most of the naphthalene mass is vaporized at a temperature below the boiling point (491 K), ΔT_{TL} appears to remain constant when similar conditions are applied. The rate of mass loss can be correlated with the same thermal-lag correlation factor for cellulose (C = 0.131 min in Model I).

Experimental and calculated conversion profiles for cellulose are compared in Figure 5 for different heating rates. For each case, only a few experimental data points were selected for the representation. The solid lines are conversion profiles estimated

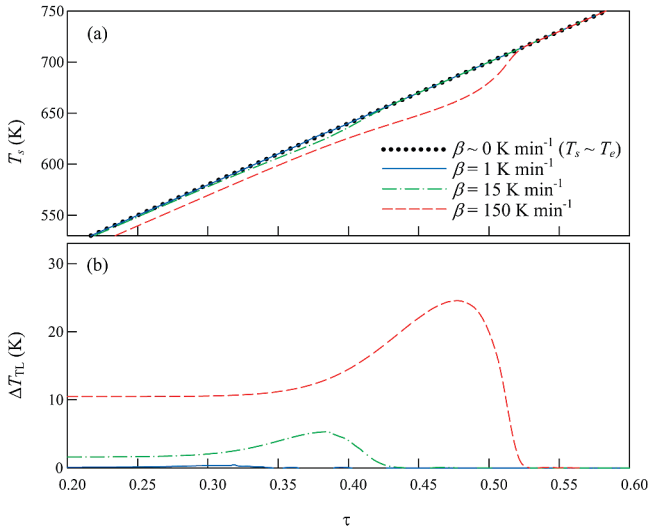

Figure 6. Effects of heating rates on (a) sample temperatures and (b) thermal-lags (estimated based on Model II).

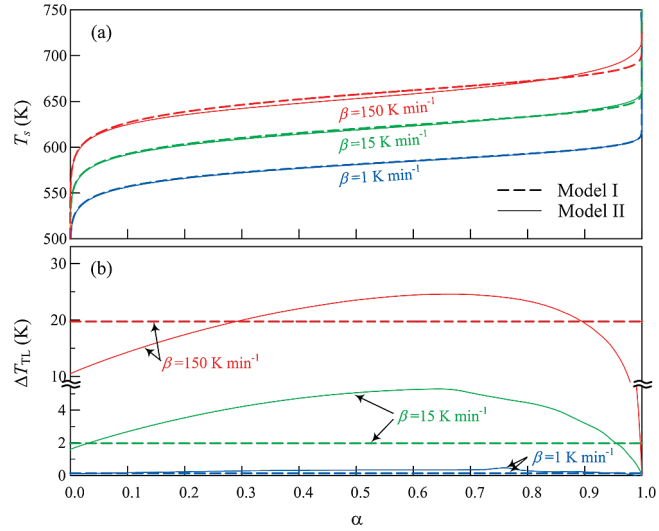

Figure 7. Estimated (a) sample temperatures and (b) thermal-lags along the mass conversion of cellulose during pyrolysis.

with the rate parameters listed in Table 4. Model estimations by both Models I and II are nearly identical and show good agreements with observed conversion profiles at different heating rates. Consistent with experimental data, the onset of pyrolysis occurs in the range of 500−600 K. For the low heating rate, most of the cellulose is pyrolyzed between 550 and 610 K with its highest conversion rate at 580 K. A faster heating rate increases both the onset of pyrolysis and the terminal temperature in which most of the cellulose is pyrolyzed. As the heating rate increases to the maximum value (150 K min^{-1}), pyrolysis of cellulose is delayed by 100 K, and overall weight loss occurs at a wider temperature range while the external temperature is linearly increased by a constant heating rate.

Figure 6 shows the effects of heating rates on estimated sample temperatures and corresponding thermal-lags. In order to compare the relative dynamic properties, the time scale is normalized with respect to the time that reaches final temperature:

$$\tau = \frac{\beta t}{T_f - T_0} \qquad (0 \le \tau \le 1) \qquad (11)$$

The external temperature (dotted line) is a linear function of τ and independent of heating rates.

Initially, sample temperature increases parallel to the external temperature. The pyrolysis does not occur in this regime so that a negligible amount of weight change is observed. With further increase of τ, sample temperature reaches the onset of chemical conversion, and the heat of endothermic pyrolysis results in an additional thermal-lag effect. At a low heating rate (1 K min^{-1}), only a trace of thermal-lag exists near $\tau = 0.3$, while the faster heating rate (150 K min^{-1}) induces a higher thermal-lag effect that indicates a large temperature difference between the sample and furnace as shown in Figure 6b. As the sample becomes nearly consumed, the thermal-lag decreases with a highly negative slope at a high heating rate. Consequently the thermal-lag effect disappears at the point that conversion reaches its plateau near $\alpha = 1$ and the sample temperature asymptotically approaches the external temperature.

Figure 7 shows the sample temperature and thermal-lag curves as a function of conversion. At each heating rate, the thermal-lag is assumed to be constant in Model I while the thermal-lag profile is estimated by the energy balance associated with the conversional rate of cellulose in Model II. The maximal deviation for high heating rates in Model II occurs at around $\alpha = 0.65$. The sample temperature curves estimated by Model I have almost identical shapes. An increase of heating rate results in vertical shifts due to the thermal-lag increase as their relationships are being implied in eq 5. It is noteworthy that estimated sample temperature profiles based on both models show only a slight difference even though each model adopts a different thermal-lag approximation. Model estimation for the sample temperature shows that the drastic pyrolysis conversion of cellulose occurs at the ranges between 520 to 610 K for 1 K min^{-1}, 550 to 660 K for 15 K min^{-1}, and 580 to 700 K for 150 K min^{-1}, respectively.

5. Discussion

5.1. Proposed Reaction Pathway. Figure 8 shows a proposed mechanism for cellulose pyrolysis based on our chemical analysis. Cellulose depolymerization begins at a moderate temperature (373−423 K). Cellulose initially decomposed to the oligosaccharides having relatively lower molecular units and continued to complete chain breaks until it reached the sugar level. The first resulting anhydro-monosaccharide is LGA. LGA can undergo dehydration and isomerization reactions to form other anhydro-monosaccharides such as DGP, LGO, and AGF. These anhydro-monosaccharides may either be repolymerized to form anhydro-oligomers[67] or further transformed by fragmentation/retroaldol condensation, dehydration, decarbonylation, or decarboxylation. Fragmentation/retroaldol condensation pathways produce hydroxyacetaldehyde, hydroxyacetone, and glyceraldehyde. It has also been proposed that these fragmented species form directly from the active cellulose. More research is needed to verify how much of these species form from LGA versus the active cellulose species. Dehydration produces water and furanoses including furfural, 5-HMF, etc. CO and CO_2 are generated by a very complex series of reactions that probably involved decarbonylation and decarboxylation, respectively.[51,52] All the products may be further converted to form char (except CO and CO_2) or be converted into light gases. Our results suggest that secondary reactions of LGA including dehydration and fragmentation occur during the pyrolysis of cellulose.

5.2. Empirical Chemistry. Most of the available carbons from cellulose pyrolysis are anhydro-monosaccharides accounting for 40% of the carbon. This is similar to recent quantification

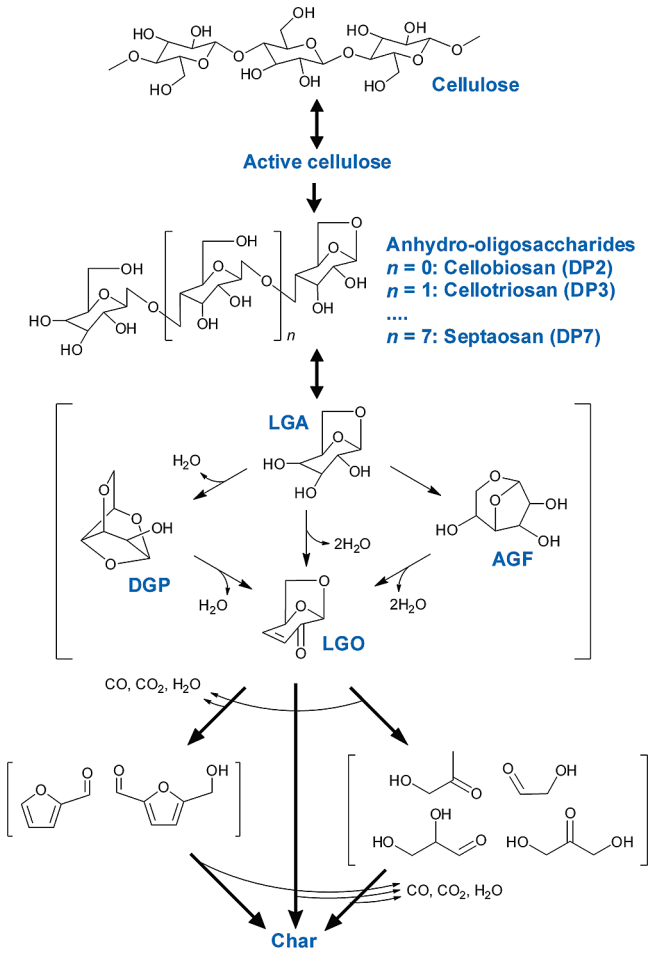

Figure 8. Proposed mechanism of cellulose pyrolysis (DP indicates 'degree of polymerization').

carried out by the Fabbri group,[68,69] who identified LGO, 1-hydroxy-3,6-dioxabicyclo[3.2.1]octane-2-one (LAC), DGP, and LGA as the major products with a 20 K min^{-1} heating rate and a final temperature at 773 K. It is noteworthy that approximately 20% of the carbon was determined in their study. It is highly plausible the missing carbons in their Py-GC-MS system are some of the anhydrosugars and anhydro-oligomers, which tend to condense inside the interface of the pyrolysis system before entering the GC-MS system due to their high boiling points. In addition, these species are thermally unstable with estimated lifetimes of less than 20 ms,[22,23] rendering secondary decomposition possible. The liquid-nitrogen trap device in the present study seems to provide an efficient way to circumvent such difficulties in collecting biomass-pyrolyzed volatiles. Importantly when we used the TGA-MS to identify products, over 30 wt % of the products were light gases including CO and CO_2. When the Pyroprobe-liquid nitrogen trap system was used, less than 18 wt % of the products were CO and CO_2. This suggests that instant quenching suppresses secondary decomposition.

A themogravimetric analysis at different transport conditions was repeated to validate that we were operating in a regime free from mass- and heat-transfer limitations. A high heating rate (150 K min^{-1}) was applied to exaggerate thermal effects for all trials: increased sample particle size reduces the relative ratio of area to volume, which may result in significant temperature and concentration gradients across the boundary. However, such influences proved insignificant in the current study. It implies that the unit size of sample did not affect thermal and mass transport characteristics associated with cellulose pyrolysis and estimated thermal-lag. The effect of sweep gas was also investigated. Higher flow rate may promote a convective heat transfer relative to conduction through the sample mass and lower a boundary layer thickness when the sample is exposed directly to the gas flow. However, no significant difference in a conversion profile was observed when different flow rates were applied to the system.

Initial sample mass has been noted to play a decisive role in deriving cellulose pyrolysis kinetics.[26,47,70,71] In Figure 2c, the deformation of the DTG peak with increasing initial cellulose mass implies existing significant temperature inhomogeneities between the outer surface and core of sample during pyrolysis. This has been observed by Lédé and associates,[23] who found a transient state (intermediate liquid compound, ILC) between the solid cellulose pellet and the external environment. During pyrolysis, a steady-state equilibrium between cellulose decomposition to ILC and ILC vaporization allows a significant temperature gradient.[20,23] This behavior explains the shift of DTG curves when increasing the initial mass of cellulose during pyrolysis. As it regards the temperature inside the cellulose particle, a uniform distribution was assumed based on the estimation of the Biot number by Piskorz and collaborators.[5] In their study, the Biot number for 180 μm cellulose particle size was less than 0.2, suggesting a uniform temperature distribution during pyrolysis. Comparatively, a 3-fold smaller diameter of particle was employed in this study, allowing a negligible Biot number; in another words, a uniform temperature distribution inside the cellulose particle was reasonable.

The similar shapes of these TG curves suggested close activation energies. However, the declining DTG curves with increasing heating rates implied thermal-lag effects.[72] Hence, thermal-lag influences should be evaluated prior to deriving the kinetics of cellulose pyrolysis. The decrease of pyrolysis residues with increase of heating rate implies changes in pyrolysis chemistry. According to Antal and co-workers,[72] the sample with the lowest heating rate was pyrolyzed below 573 K for a significant period of time, forming considerable amounts of char precursors such as mono- and oligomer type products. This explains the slightly higher char yield for cellulose pyrolysis in the lowest heating rate (1 K min^{-1}) in Figure 3a.

5.3. Comparison to Literature Mechanisms. The tiny endothermic peaks at around 475 K for low and moderate heating rates were originally proposed as the dehydration step in cellulose pyrolysis.[73] However, neither weight loss nor MS responses indicated this dehydration step in this study. Later, Shafizadeh and collaborators[38,74] proposed an "active cellulose" stage, a glass transient/depolymerization of cellulose that reduces molecular weight from 2500 (virgin cellulose) to 200. The step was suggested as the initiation prior to further cellulose decomposition, though the Antal group questioned it.[72] The post-run cellulose in the present study displayed a significant color change: from its original white to yellowish, implying altered cellulose. In addition, the repeated-trial shown in Figure 4 highlighted that this initiation is reproducible. Our X-ray diffraction patterns (not presented) also indicated no crystalline deformation for pre- and post-treated cellulose. It is, therefore, highly possible that part of the scission bonds may be rebuilt without further heat input, in contradiction to Diebold's proposed mechanism (Scheme 1),[75] which suggests the active cellulose has a great tendency to transform into char without further cleavage and heat input. CO_2 also suggests a picture different than that of the Diebold model for cellulose pyrolysis.[75] The CO_2 signal was first detected at approximately 500 K, which

SCHEME 1: Global Cellulose Pyrolysis Scheme Proposed by Diebold[75]

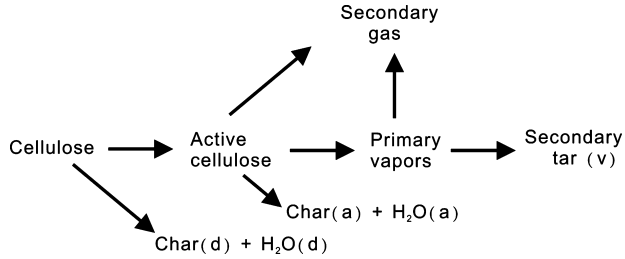

would be at the temperature where Diebold proposed active cellulose with no CO_2 being formed.

We propose here a model for cellulose pyrolysis different than that of the Diebold mechanism.[75] Diebold's model involves cellulose first forming an active cellulose species that then undergoes three parallel pathways to form char, secondary gas, or primary vapors as shown as Scheme 1. The primary vapors can then undergo further reaction to form secondary gas and char. Our model is described in Figure 8 in Section 5.1 and consists of a number of series reaction pathways. In contrast to having three parallel pathways, our model suggests that cellulose decomposes to form anhydrosugar or sugar polymers. These anhydrosugars can then undergo a series of different reactions.

We believe our kinetic model is more physically realistic than Diebold's model for several reasons. First, we are able to pyrolyze over 95 wt % of the cellulose with very little char formation in a dynamic TGA-DSC system. This indicates that the majority of the char does not form from the "active cellulose." Instead we propose the majority of the char forms from repolymerization of the volatile anhydrosugar and fragmented species. If the concentration of these anhydrosugar remains high then char will form. However, we recognize that char may form directly from cellulose particularly at low temperatures (less than 573 K).[74] It should be noted that the char formation in the Pyroprobe was significantly higher than the char formed in the TGA. In the Pyroprobe reactor we obtain higher concentration of the volatile products than that in the TGA because no sweep gas is introduced into the pyrolysis zone of the Pyroprobe reactor. This higher concentration of volatiles may explain why more coke is observed in the Pyroprobe reactor.

We are able to obtain high yields of anhydrosugars by quickly trapping them out. This most likely indicates that they are the first product from cellulose pyrolysis. The light gases (including CO, and H_2O) are formed after cellulose weight decreases as shown in our TGA-MS experiments in Figure 3d. When char is formed, water must also be formed. This implies under our experimental conditions that char is not originated from a parallel pathway of "active cellulose." Clearly more research is needed to understand the mechanisms of char formation from cellulose pyrolysis.

Generally, increasing heating rates shifts the occurrence of pyrolysis to higher temperatures. However, for the three heating rates employed, similar char yields were observed (6.3, 6.1, and 4.6 wt % for 1, 15, and 150 K min^{-1}, respectively). With faster heating rates, there is less char formation. Compared to the initial mass, the residue (i.e., char) for each trial is negligible ($m_f/m_0 < 0.01$). Hence, our proposed model neglects char formation by parallel pathways which probably only occurs at a sufficiently slow heating rate; $\beta \ll 1$ K min^{-1} or low temperatures.

Cellulose pyrolysis models have been intensively surveyed and revisited since the well-known B−S model was proposed (Appendix A). Nevertheless, most of these models are "global pyrolysis schemes," by which products are lumped into three or four phases, such as gases, tar, char, and active cellulose in some cases. A molecular-based cellulose pyrolysis mechanism is currently absent. Evans and Milne[76] showed the chemistry of cellulose decomposition to anhydrosugars. Recently, the Fabbri group[68,69] provided a mechanism of how the anhydromonosaccharides interacted and evolved during cellulose pyrolysis. It is our belief that a major goal of pyrolysis research should be to try and develop a mechanistically based kinetic model for cellulose pyrolysis.

5.4. Kinetic Modeling. Our results are consist with Antal et al.[47] who have indicated that the shift of pyrolytic temperature for different heating rates is due to thermal-lag effects. Grønli et al.[49] reported a round-robin study which includes kinetic observations of cellulose pyrolysis individually obtained from seven thermogravimetric systems at similar operating conditions. In their fit of a first-order reaction model to experimental data, the activation energy varied in a range between 234−263 kJ mol^{-1} and the pre-exponential factor was between $10^{17.8}$ and $10^{21.1}$ s^{-1}. Measured temperature profiles for cellulose pyrolysis shows a systematic behavior for different heating rates (5 and 40 K min^{-1}). It seems to depend on the intrinsic factors of the system rather than operating conditions, which are almost identical in this comparison (Figures 2 and 3 in ref 49).

Consistent with such experimental results, some other authors[65,77] have adopted a mathematical approach to correlate systematic thermal-lag patterns of experimental TGA data in their polymer kinetic studies. Chiu et al.[77] corrected the thermal-lag properties of different cooling rates for polystyrene using a standard material (indium). Hieber[78] explicitly introduced the thermal-lag correlation factor which has the same value as the previous results of Manasse and Haudin.[65] This method is analogous to the thermal-lag approach in our Model I. In the thermal-lag relation of eq 5, the actual sample temperature is lower than the measured external temperature by $C\beta$ (in K). As shown in Figure 5, the simple thermal-lag expression with a single parameter provides an excellent correlation for the thermal-lag behaviors for different heating rates, especially in the region of conversion below 95%. By lowering the heating rates, the sample temperature asymptotically approaches the equilibrium temperature if the single reaction mechanism is assumed. However, the model overestimates actual weight loss near complete conversion. Numerically, a model for the first-order reaction rate cannot be used to further improve fitting for this regime. A thermal-lag model combined with the reaction kinetics is an effective approach to fit TGA data.

At a high heating-rate condition, a large thermal gradient can be present around the sample boundary. As the pyrolytic conversion increases, the sample mass decreases which lowers the thermal-lag. With the current presumption of nonisothermal state of a DSC-TGA system, Model II employs the overall energy balance that couples reaction heat, heat exchange through sample surface, and the sensible heat demand by remaining sample mass. In this approach, it is assumed that the amount of heat transferred to the sample is equal to the sum of heat demands of the sample temperature increase and heat requirement involved in an endothermic pyrolysis. This energy-balance-based model is physically more meaningful than Model I but demands accurate thermophysical parameters, which should be determined separately. In addition, it is computationally more expensive. However, both models give similar fits to the data.

In summary, we believe that Model I, which is relatively more simple and independent of thermophysical properties of samples

(Table 3), provides a reasonable approach to the estimation of rate parameters for the pyrolytic conversion of biomass derived material inside a TGA.

6. Conclusion

The kinetics and mechanism of cellulose pyrolysis were studied. A newly designed approach was employed to capture the vaporized products during cellulose pyrolysis. In order to identify the chemical species, the resulting samples were analyzed by both GC-MS and LC-MS. The speciation and kinetic behaviors are in agreement with the literature, while the quantification of carbon-containing products was greatly improved. Nearly 90% of the carbon can be quantified. The first step involved in cellulose pyrolysis occurs at a temperature of 475 K and involves reactions within the solid cellulose. This reaction, which is similar to the formation of active cellulose proposed by other researchers is shown to be reversible. Cellulose pyrolysis yields LGA and anhydrosugar polymers. LGA can undergo isomerization and dehydration reactions to form other anhydro-monosaccharides. The anhydro-monosaccharides can polymerize, undergo dehydration reactions, and undergo retroaldol condensation reactions. Polymerization of the anhydrosugars results in the formation of oligomers. Dehydration of the anhydrosugars forms furanoses. Retroaldol condensation of anhydrosugars form hydroxyacetaldehyde, hydroxyacetone, and glyceraldehyde. CO and CO_2 are formed by decarbonylation and decarboxylation. Thermogravimetric analysis was also carried out to measure the dynamic behavior of cellulose pyrolysis. The overall pyrolytic conversion of cellulose was governed by a first-order endothermic reaction. When a faster heating rate applied to cellulose decomposition, a greater thermal-lag was observed. The reaction models coupled to two thermal-lag estimations were used to adjust observed cellulose pyrolytic conversion, and the best overall fit value was obtained at $\log(k_0) = 14.8$ and $E = 198$ kJ mol^{-1}. Importantly, we show here that the kinetics of cellulose pyrolysis are not a function of heating rate. The current study provides an improved kinetic model of cellulose pyrolysis to LGA.

Appendix

Nomenclature

AGF	1,6-anhydro-β-D-glucofuranose(2,8-dioxabicyclo[3.2.1]octane-4,6,7-triol)
A_r	surface area of spherical sample, m^2
c_p	heat capacity of cellulose, J kg^{-1} K^{-1}
C	thermal-lag correction factor, min
DGP	1,4:3,6-dianhydro-β-D-glucopyranose
DSC	differential scanning calorimetry
DTG	derivative thermogravimetric
E_A	activation energy, J mol^{-1}
F	object function for parameter estimation
GC	gas chromatography
HMF	hydroxymethylfurfural (5-(hydroxymethyl)furan-2-carbaldehyde)
HPLC	high performance liquid chromatography
h	heat-transfer coefficient, J s^{-1} m^{-2} K^{-1}
ILC	intermediate liquid compound
k	first-order reaction rate constant, s^{-1}
k_o	pre-exponential or frequency factor, s^{-1}
LAC	δ-lactone of 3-hydroxy-5-hydroxymethyltetrahydrofuran-3-carboxylic acid (1-hydroxy-3,6-dioxabicyclo[3.2.1]octan-2-one)
LGA	levoglucosan (6,8-dioxabicyclo[3.2.1]octane-2,3,4-triol)
LGO	levoglucosenone (6,8-dioxabicyclo[3.2.1]oct-2-en-4-one)
MS	mass spectrometry
m_o	initial weight of dried cellulose, g
m_f	final weight of residue after cellulose pyrolysis, g
t	time, s
TGA	thermogravimetric analysis
T_e	external temperature, K
T_f	final temperature, K
T_o	initial temperature, K
T_s	sample temperature, K

Greek Symbols

α	pyrolytic conversion of cellulose
β	heating rate, K min^{-1} and K s^{-1}
$\Delta\alpha$	change of solution vector during the iteration of parameter-searching algorithm
$\Delta\mathbf{F}$	change of object function during the iteration of parameter-searching algorithm
ΔH	heat of cellulose pyrolysis, J g^{-1}
ΔT_{TL}	thermal-lag, K
ε	convergence criterion
τ	dimensionless time

Acknowledgment. This work was supported by the National Science Council (Taiwan) under Project NSC-096-2917-I-564-114, a National Science Foundation-Major Research Instrumentation Program (NSF-MRI) grant, and by the Defense Advanced Research Project Agency (DARPA) through the Defense Science Office Cooperative Agreement W911NF-09-2-0010 (Surf-cat: Catalysts for production of JP-8 range molecules from lignocellulosic biomass). Mass spectral data were obtained at University of Massachusetts Mass Spectrometry Facility which is supported, in part, by the National Science Foundation. This work was approved for public release by DARPA Technical Information Office, distribution unlimited.

Supporting Information Available: Appendix A represents the summary of cellulose pyrolysis models. This information is available free of charge via the Internet at http://pubs.acs.org.

References and Notes

(1) Klass, D. L. *Biomass for Renewable Energy, Fuels, and Chemicals*; Academic Press: San Diego, 1998.
(2) Bridgwater, A. V.; Meier, D.; Radlein, D. *Org. Geochem.* **1999**, *30*, 1479.
(3) Bridgwater, A. V. *Chem. Eng. J.* **2003**, *91*, 87.
(4) Wang, D.; Czernik, S.; Montane, D.; Mann, M.; Chornet, E. *Ind. Eng. Chem. Res.* **1997**, *36*, 1507.
(5) Piskorz, J.; Majerski, P.; Radlein, D.; Vladars-Usas, A.; Scott, D. S. *J. Anal. Appl. Pyrolysis* **2000**, *56*, 145.
(6) Brown, A. L.; Dayton, D. C.; Nimlos, M. R.; Daily, J. W. *Energy Fuels* **2001**, *15*, 1276.
(7) Brown, A. L.; Dayton, D. C.; Daily, J. W. *Energy Fuels* **2001**, *15*, 1286.
(8) Mohan, D.; Pittman, C. U.; Bricka, M.; Smith, F.; Yancey, B.; Mohammad, J.; Steele, P. H.; Alexandre-Franco, M. F.; Gomez-Serrano, V.; Gong, H. *J. Colloid Interface Sci.* **2007**, *310*, 57.
(9) Mohan, D.; Shi, J.; Nicholas, D. D.; Pittman, C. U.; Steele, P. H.; Cooper, J. E. *Chemosphere* **2008**, *71*, 456.
(10) Pletka, R.; Brown, R. C.; Smeenk, J. *Biomass Bioenergy* **2001**, *20*, 297.
(11) Pletka, R.; Brown, R. C.; Smeenk, J. *Biomass Bioenergy* **2001**, *20*, 307.
(12) Merida, W.; Maness, P. C.; Brown, R. C.; Levin, D. B. *Int. J. Hydrogen Energy* **2004**, *29*, 283.
(13) Zhang, R. Q.; Brown, R. C.; Suby, A. *Energy Fuels* **2004**, *18*, 251.
(14) Elliott, D. C. *Biofuels Bioprod. Biorefining* **2008**, *2*, 254.

(15) Carlson, T. R.; Vispute, T. P.; Huber, G. W. *ChemSusChem* **2008**, *1*, 397.
(16) Carlson, T. R.; Tompsett, G. A.; Conner, W. C.; Huber, G. W. *Top. Catal.* **2009**, *52*, 241.
(17) Mohan, D.; Pittman, C. U.; Steele, P. H. *Energy Fuels* **2006**, *20*, 848.
(18) Bridgwater, A. V.; Peacocke, G. V. C. *Renewable Sustainable Energy Rev.* **2000**, *4*, 1.
(19) Czernik, S.; Bridgwater, A. V. *Energy Fuels* **2004**, *18*, 590.
(20) Mamleev, V.; Bourbigot, S.; Le Bras, M.; Yvon, J. *J. Anal. Appl. Pyrolysis* **2009**, *84*, 1.
(21) Lanza, R.; Dalle Nogare, D.; Canu, P. *Ind. Eng. Chem. Res.* **2009**, *48*, 1391.
(22) Lédé, J.; Blanchard, F.; Boutin, O. *Fuel* **2002**, *81*, 1269.
(23) Boutin, O.; Ferrer, M.; Lédé, J. *Chem. Eng. Sci.* **2002**, *57*, 15.
(24) Narayan, R.; Antal, M. J. *Ind. Eng. Chem. Res.* **1996**, *35*, 1711.
(25) Di Blasi, C. *Ind. Eng. Chem. Res.* **1996**, *35*, 37.
(26) Volker, S.; Rieckmann, T. *J. Anal. Appl. Pyrolysis* **2002**, *62*, 165.
(27) Stamm, A. *Ind. Eng. Chem.* **1956**, *48*, 413.
(28) Chatterjee, P. *Text. Res. J.* **1966**, *36*, 487.
(29) Tang, W. K. U.S. *For. Serv. Res. Pap. FPL* **1967**, 71.
(30) Lipska, A. E.; Frank, A. Wodley. *J. Appl. Polym. Sci.* **1969**, *13*, 851.
(31) Fung, D. P. C. *Tappi* **1969**, *52*, 319.
(32) Roberts, A. F. *J. Appl. Polym. Sci.* **1970**, *14*, 244.
(33) Kanury, A. M. *Combust. Flame* **1972**, *18*, 75.
(34) Hirata, T. *Ringyo Shikenjo Kenkyu Hokoku* **1974**, *263*, 1.
(35) Baker, R. R. *J. Therm. Anal.* **1975**, *8*, 163.
(36) Lewellen, P.; Peters, W. A.; Howard, J. B. 16th International Symposium on Combustion, (MIT, Cambridge, Massachusetts, August 15-20, 1976) Combustion Institute: Pittsburgh, PA, 1977, p. 1741–1780.
(37) Min, K. *Combust. Flame* **1977**, *30*, 285.
(38) Bradbury, A. G. W.; Sakai, Y.; Shafizadeh, F. *J. Appl. Polym. Sci.* **1979**, *23*, 3271.
(39) Antal, M. J.; Friedman, H. L.; Rogers, F. E. *Combust. Sci. Technol.* **1980**, *21*, 141.
(40) Hajaligol, M.; Howard, J.; Longwell, J.; Peters, W. *Ind. Eng. Chem. Process Des. Dev.* **1982**, *21*, 457.
(41) Várhegyi, G.; Antal, M. J.; Szekely, T.; Szabo, P. *Energy Fuels* **1989**, *3*, 329.
(42) Várhegyi, G.; Szab, P.; Antal, M. J. *Biomass Bioenergy* **1994**, *7*, 69.
(43) Font, R.; Marcilla, A.; Garcia, A. N.; Caballero, J. A.; Conesa, J. A. *J. Anal. Appl. Pyrolysis* **1995**, *32*, 29.
(44) Conesa, J. A.; Caballero, J. A.; Marcilla, A.; Font, R. *Thermochim. Acta* **1995**, *254*, 175.
(45) Milosavlevic, I.; Suuberg, E. *Ind. Eng. Chem. Res.* **1995**, *34*, 1081.
(46) Aggarwal, P.; Dollimore, D.; Heon, K. *J. Therm. Anal. Calorim.* **1997**, *50*, 7.
(47) Antal, M. J.; Várhegyi, G.; Jakab, E. *Ind. Eng. Chem. Res.* **1998**, *37*, 1267.
(48) Rao, T. R.; Sharma, A. *Energy* **1998**, *23*, 973.
(49) Grønli, M.; Antal, M. J.; Várhegyi, G. *Ind. Eng. Chem. Res.* **1999**, *38*, 2238.
(50) Banyasz, J. L.; Li, S.; Lyons-Hart, J. L.; Shafer, K. H. *J. Anal. Appl. Pyrolysis* **2001**, *57*, 223.
(51) Mamleev, V.; Bourbigot, S.; Yvon, J. *J. Anal. Appl. Pyrolysis* **2007**, *80*, 141.
(52) Mamleev, V.; Bourbigot, S.; Yvon, J. *J. Anal. Appl. Pyrolysis* **2007**, *80*, 151.
(53) Hirata, T.; Maekawa, M.; Nohmi, T. *J. Mass Spectrom. Soc. Jpn.* **1998**, *46*, 259.
(54) Broido, A.; Weinstein, M. Kinetics of solid-phase cellulose pyrolysis. In 3rd International Conference of Thermal Analysis, Wiedemann, I., Ed.; Birkhauser Verlag: Basel, 1971; p 285.
(55) Milosavljevic, I.; Oja, V.; Suuberg, E. *Ind. Eng. Chem. Res.* **1996**, *35*, 653.
(56) Suuberg, E.; Milosavljevic, I.; Oja, V. *Symp. (Int.) Combust. [Proc.]* **1996**, *26*, 1515.
(57) Soravia, D. R.; Canu, P. *Ind. Eng. Chem. Res.* **2002**, *41*, 5990.
(58) Demirbas, A.; Arin, G. *Energy Sources* **2002**, *24*, 471.
(59) Reynolds, J. G.; Burnham, A. K. *Energy Fuels* **1997**, *11*, 88.
(60) Li, S.; Lyons-Hart, J.; Banyasz, J.; Shafer, K. *Fuel* **2001**, *80*, 1809.
(61) Banyasz, J. L.; Li, S.; Lyons-Hart, J.; Shafer, K. H. *Fuel* **2001**, *80*, 1757.
(62) Piskorz, J.; Peacocke, G. V. C.; Bradbury, A. G. W. IEA Pyrolysis Fundamentals Review: Active Research Groups Appended. In *Fast Pyrolysis of Biomass: A Handbook*; Bridgwater, A. V., Czernik, S., Diebold, J. P., Meier, D., Oasmaa, A., Peacocke, G. V. C., Piskorz, J., Radlein, D., Eds.; CPL Press: Newbury, 2002; p 14.
(63) Shafizadeh, F.; Bradbury, A. G. W. *J. Appl. Polym. Sci.* **1979**, *23*, 1431.
(64) Focher, B.; Palma, M. T.; Canetti, M.; Torri, G.; Cosentino, C.; Gastaldi, G. *Ind. Crop Prod.* **2001**, *13*, 193.
(65) Monasse, B.; Haudin, J. M. *Colloid Polym. Sci.* **1986**, *264*, 117.
(66) Cooley, S.; Antal, M. J. *J. Anal. Appl. Pyrolysis* **1988**, *14*, 149.
(67) Kawamoto, H.; Murayama, M.; Saka, S. *J. Wood Sci.* **2003**, *49*, 469.
(68) Fabbri, D.; Torri, C.; Mancini, I. *Green Chem.* **2007**, *9*, 1374.
(69) Fabbri, D.; Torri, C.; Baravelli, V. *J. Anal. Appl. Pyrolysis* **2007**, *80*, 24.
(70) Antal, M. J.; Várhegyi, G. *Ind. Eng. Chem. Res.* **1995**, *34*, 703.
(71) Antal, M. J.; Grønli, M. *Ind. Eng. Chem. Res.* **2003**, *42*, 1619.
(72) Várhegyi, G.; Antal, M. J.; Jakab, E.; Szab, P. *J. Anal. Appl. Pyrolysis* **1997**, *42*, 73.
(73) Kilzer, F. J.; Broido, A. *Pyrodynamics* **1965**, *2*, 151.
(74) Shafizadeh, F.; Fu, Y. L. *Carbohydr. Res.* **1973**, *29*, 113.
(75) Diebold, J. P. *Biomass Bioenergy* **1994**, *7*, 75.
(76) Evans, R. J.; Milne, T. A. *Energy Fuels* **1987**, *1*, 123.
(77) Chiu, F.-C.; Peng, C.-G.; Fu, Q. *Polym. Eng. Sci.* **2000**, *40*, 2397.
(78) Hieber, C. A. *J. Appl. Polym. Sci.* **2004**, *91*, 2402.

JP906702P